Continental Shelf Research 108 (2015) 55–64

Contents lists available at ScienceDirect

Continental Shelf Research

journal homepage: www.elsevier.com/locate/csr

Evolution of a physical and biological front from upwelling to relaxation

Yanwu Zhang [a,*], James G. Bellingham [b], John P. Ryan [a], Michael A. Godin [c]

[a] Monterey Bay Aquarium Research Institute, CA, USA
[b] Woods Hole Oceanographic Institution, MA, USA
[c] IntuAware, MA, USA

ARTICLE INFO

Article history:
Received 19 December 2014
Received in revised form
30 July 2015
Accepted 7 August 2015
Available online 8 August 2015

Keywords:
Fronts
Upwelling
Relaxation
Autonomous underwater vehicle

ABSTRACT

Fronts influence the structure and function of coastal marine ecosystems. Due to the complexity and dynamic nature of coastal environments and the small scales of frontal gradient zones, frontal research is difficult. To advance this challenging research we developed a method enabling an autonomous underwater vehicle (AUV) to detect and track fronts, thereby providing high-resolution observations in the moving reference frame of the front itself. This novel method was applied to studying the evolution of a frontal zone in the coastal upwelling environment of Monterey Bay, California, through a period of variability in upwelling intensity. Through 23 frontal crossings in four days, the AUV detected the front using real-time analysis of vertical thermal stratification to identify water types and the front between them, and the vehicle tracked the front as it moved more than 10 km offshore. The physical front coincided with a biological front between strongly stratified phytoplankton-enriched water inshore of the front, and weakly stratified phytoplankton-poor water offshore of the front. While stratification remained a consistent identifier, conditions on both sides of the front changed rapidly as regional circulation responded to relaxation of upwelling winds. The offshore water type transitioned from relatively cold and saline upwelled water to relatively warm and fresh coastal transition zone water. The inshore water type exhibited an order of magnitude increase in chlorophyll concentrations and an associated increase in oxygen and decrease in nitrate. It also warmed and freshened near the front, consistent with the cross-frontal exchange that was detected in the high-resolution AUV data. AUV-observed cross-frontal exchanges beneath the surface manifestation of the front emphasize the importance of AUV synoptic water column surveys in the frontal zone.

1. Introduction

Fronts are ubiquitous features of eastern boundary upwelling systems. Monterey Bay, California (Fig. 1) lies in the eastern boundary upwelling system of the northeastern Pacific, the California Current System (CCS). As in other eastern boundary current systems, wind-forced upwelling in the CCS enhances the supply of nutrients to the euphotic zone and associated primary productivity (Barber and Smith, 1981; Pennington and Chavez, 2000). In the Monterey Bay region, upwelling centers are linked to coastal land features north and south of the bay (Rosenfeld et al., 1994; Breaker and Broenkow, 1994; Ramp et al., 2005), at Point Año Nuevo and Point Sur (Fig. 1). A prominent ecological feature, the upwelling shadow of northern Monterey Bay (Graham et al., 1992; Breaker and Broenkow, 1994), was originally recognized for its relatively warm, stratified water and diverse plankton community that contrasted sharply with cold, weakly stratified and plankton-poor water transported southward across the mouth of the bay from the Point Año Nuevo upwelling center. The relatively long residence time and enhanced stratification of the upwelling shadow (Graham and Largier, 1997), coupled with episodic nutrient fluxes into it, support its role as an incubator of different types of phytoplankton blooms, including harmful algal species (Ryan et al., 2008a, 2010a, 2011, 2014a,b; Jessup et al., 2009).

Fronts along the boundaries of the Año Nuevo upwelling plume have been linked to a variety of ecological consequences. Along the eastern front of this upwelling plume, i.e., the upwelling shadow front, convergent circulation is prevalent (Woodson et al., 2009; Ryan et al., 2010a), and internal waves are generated by variable wind forcing (Woodson et al., 2011). Frontal influences on phytoplankton include local enhancement of nutrient supply,

* Corresponding author.
E-mail address: yzhang@mbari.org (Y. Zhang).

http://dx.doi.org/10.1016/j.csr.2015.08.005

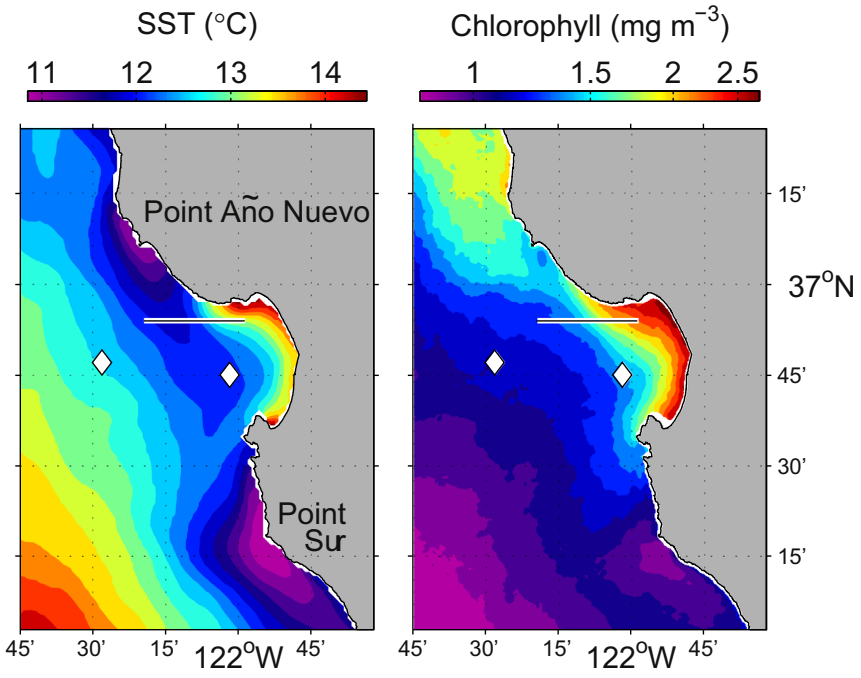

Fig. 1. Sea surface temperature (SST) (left panel) and sea surface chlorophyll concentration (right panel) in June (averaged from 2004 to 2008) in Monterey Bay. The NDBC (National Data Buoy Center) buoy #46042 and the M1 mooring are marked by the left and right diamonds, respectively. An AUV tracked a front on the 36.9°N latitude (black line) in June 2012 (see Sections 2 and 3). (For interpretation of color in this figure, the reader is referred to the web version of this paper.)

accumulation of biomass in the front, and shear induced formation of thin layers (Ryan et al., 2008b, 2010a,b). Enhanced abundances of microzooplankton have also been observed in this front (Harvey et al., 2012). Both the eastern and western fronts of this upwelling plume have been shown to control patterns of recruitment in coastal reef fish and community building invertebrates of the intertidal zone (Woodson et al., 2009, 2012). At higher trophic levels, accumulation of large gelatinous zooplankton has been observed (Graham et al., 1992), and densely concentrated patches of acoustic scatterers have been detected, interpreted to be small pelagic fish schools (J. Figurski, unpublished data).

While fronts are critical to ecosystem structure and function, studies of frontal processes and ecology are challenging due to their complexity, dynamic nature, and the relatively small spatial scales across which frontal gradients extend. Effective research methods include multidisciplinary in situ observation of the water column, made at high-resolution in space and time. Autonomous recognition of fronts and their adjacent water types enables such observation, as well as tracking of these dynamic habitats. Using methods recently developed for this purpose, made operational on a long-range autonomous underwater vehicle (AUV) (Zhang et al., 2012a), this study provides the first detailed examination of biogeochemical variability across the ecologically significant Monterey Bay upwelling shadow front during a transition from wind-driven upwelling to relaxation.

2. Methods

2.1. Tethys long-range AUV

The Tethys long-range AUV (Bellingham et al., 2010b) is a propeller-driven vehicle that can run at a speed between 0.5 and 1 m/s. It has a length of 2.3 m and a diameter of 0.3 m at the midsection. Propulsion power consumption is minimized through designs of a low-drag body and a high-efficiency propulsion system. By also using a buoyancy engine, the vehicle is capable of ballasting to neutral buoyancy and flying with zero angle of attack, thus further reducing drag. To conserve power, any sensor or motor controller not commanded to operate is powered off. The AUV's design range is 3000 km. The vehicle has thus far demonstrated 1800 km range through a 23-day mission off the California coast (Hobson et al., 2012).

The AUV's sensor suite includes Neil Brown temperature and conductivity sensors, a Keller depth sensor, WET Labs ECO-Triplet Puck fluorescence/backscatter sensors, an Aanderaa dissolved oxygen sensor, an In Situ Ultraviolet Spectrophotometer (ISUS) nitrate sensor, and a LinkQuest Doppler velocity log (DVL) of model NavQuest 600 Micro. The AUV's underwater navigation is by DVL-aided dead reckoning. The DVL provides the earth-referenced velocity of the AUV when the ocean bottom is within range (110 m). The vehicle's estimated speed is combined with measured heading and attitude and then accumulated to provide the estimated location of the AUV. The vehicle periodically ascends to the surface for a global positioning system (GPS) fix to correct the AUV's underwater navigation error (Bellingham et al., 2010a).

2.2. AUV front tracking algorithm

We have developed algorithms for an AUV to autonomously distinguish between relatively strongly and weakly stratified water columns and accordingly detect the front between the two water types (Zhang et al. 2012a,b). In the strongly stratified water column, the vertical temperature difference between shallow and deep depths is large (warm at surface and cold at depth). In the weakly stratified water column, the vertical temperature difference is small. On each descent or ascent profile on the AUV's sawtooth (i.e., yo–yo) trajectory (in the vertical dimension), the vehicle calculates in real time the "vertical temperature homogeneity index (VTHI)" of the water column, defined as follows (Zhang et al., 2012b):

$$\Delta Temp_{vert} = \frac{1}{N}\Sigma_{i=1}^{N}\left|Temp_{depth\_i} - \frac{1}{N}\Sigma_{i=1}^{N}Temp_{depth\_i}\right| \quad (1)$$

where i is the depth index, and N is the total number of depths included in the calculation. $Temp_{depth\_i}$ is the temperature at the ith depth. $(1/N)\Sigma_{i=1}^{N} Temp_{depth\_i}$ is the mean temperature. $\left|Temp_{depth\_i} - (1/N)\Sigma_{i=1}^{N} Temp_{depth\_i}\right|$ measures the difference (absolute value) between the temperature at each individual depth and the mean temperature. The average difference $\Delta Temp_{vert}$ (averaged over all participating depths) is a measure of the vertical homogeneity of temperature in the water column.

The AUV tracks the front autonomously as follows (Zhang et al., 2012a). Suppose an AUV starts from the strongly stratified water column (where $\Delta Temp_{vert}$ is large), flying towards the weakly stratified water column (where $\Delta Temp_{vert}$ is small) on a yo–yo trajectory (in the vertical dimension). When $\Delta Temp_{vert}$ falls below a threshold $thresh_{\Delta Temp}$ for M consecutive yo–yo profiles, the vehicle determines that it has passed the front and entered the weakly stratified water column. To avoid false detection due to measurement noise or existence of isolated water patches, the algorithm only sets the detection flag when $\Delta Temp_{vert}$ meets the threshold for M consecutive yo–yo profiles. The AUV continues flight in the weakly stratified water for some distance so as to sufficiently survey the frontal zone and this water type, and then reverses course to fly back to the strongly stratified water. On the AUV's flight toward the strongly stratified water, when $\Delta Temp_{vert}$ rises above $thresh_{\Delta Temp}$ for M consecutive yo–yo profiles, the AUV determines that it has passed the front and entered the strongly stratified water column. The AUV continues flight in this water type for some distance, and then reverses course to fly back to the weakly stratified water. The AUV repeats the above cycle, thus effectively tracking the front as the front moves over time. The AUV mission terminates once the prescribed mission duration has elapsed, and front tracking can be continued by starting a new mission with the same behavior.

2.3. Field deployment in Monterey Bay in June 2012

The algorithm was deployed on the Tethys AUV from 8 to 12 June 2012 to study the front that forms along the periphery of the Monterey Bay upwelling shadow. The AUV flew on a yo–yo trajectory between surface and 50 m depth on latitude 36.9°N, at an average horizontal speed of about 0.9 m/s and an average vertical speed of 0.24 m/s. During most of the AUV mission the seabed was out of the DVL's bottom-lock range, so the vehicle used speed estimate and measured heading and attitude to estimate its underwater location. The vehicle's dead-reckoning navigation error due to the compass error was about 2% distance traveled. The AUV periodically (about every hour) ascended to surface to obtain GPS fixes.

The 36.9°N latitude was selected based on multi-year satellite SST and chlorophyll fluorescence line height data for the month of June that showed high horizontal gradients between the upwelling filament and the upwelling shadow (see Fig. 1). Running the AUV on this latitude provided a relatively high probability of encountering strongly contrasting water types across an upwelling front (Ryan, 2011; Zhang et al., 2012b).

Previous temperature measurements in Monterey Bay indicated that $\Delta Temp_{vert}$ (in Eq. (1)) between 5 m and 30 m depths provided a strong contrast between upwelling and strongly stratified water columns. Hence we designated four participating depths for calculating $\Delta Temp_{vert}$: 5 m, 10 m, 20 m, and 30 m. We set the classification threshold $thresh_{\Delta Temp} = 0.3$ °C, also based on previous AUV temperature measurements in Monterey Bay. We set M (the number of consecutive yo–yo profiles required to meet the classification condition for robust front detection) to 5. After detecting the front, the AUV was to continue flight for 4 km to sufficiently cover the frontal zone, and then turn back to the other water type.

The Tethys AUV's temperature, conductivity, nitrate, and dissolved oxygen data were corrected using the best available references as follows. (1) *Temperature*: using a factory-provided correction based on post-deployment calibration of the AUV's Neil Brown temperature sensor, with a factory-specified accuracy of 0.0005 °C. (2) *Conductivity*: referenced to measurements by a regularly calibrated Sea-Bird SBE 4C conductivity sensor on another AUV Dorado, with a factory-specified accuracy of 0.0003 S/m. The Dorado AUV's SBE 4C conductivity sensor measurement is also compared with the measurement by an SBE 37-SM MicroCAT sensor in the test tank of the Monterey Bay Aquarium Research Institute during Dorado's pre-deployment tests, and their measurements match very well. (3) *Nitrate*: referenced to lab analysis results of the Niskin bottle water samples, with an accuracy of 2%. (4) *Dissolved oxygen*: referenced to measurements by a calibrated Sea-Bird SBE43 dissolved oxygen sensor on the CTD-rosette on R/V Fulmar, with an accuracy of 1%. For chlorophyll, we used the measurements by the Tethys AUV's factory-calibrated WET Labs ECO-Triplet Puck, with a factory-specified sensitivity of 0.015 μg/L.

2.4. Ancillary environmental data

To provide greater temporal context for the Tethys AUV observations, we examined time series of meteorological and oceanographic variability measured at regional moorings (locations shown in Fig. 1). The NDBC buoy #46042 provided hourly measurements of wind speed and direction (from NOAA website http://www.ndbc.noaa.gov/station_history.php?station=46042), key to understanding variability in upwelling forced by regional winds. The M1 Mooring provided hourly measurements of water column temperature and salinity (from MBARI website http://dods.mbari.org/data/ssdsdata/deployments/m1/201202/), key to understanding oceanographic responses in the region of outer Monterey Bay, where the AUV observations were targeted. The sensors on these moorings have been previously described (Ryan et al., 2008b). To focus on variability caused by regional wind forcing, the hourly time series from the M1 mooring was low-pass filtered using the PL33 filter (Beardsley et al., 1985), which effectively excludes diurnal and tidal signals.

Synoptic descriptions of regional SST and ocean color from satellite remote sensing were examined as context for the AUV frontal tracking and observation. Advanced Very High Resolution Radiometer (AVHRR) SST images were obtained from NOAA CoastWatch; processing methods are described in Ryan et al. (2010a). Regional ocean color data from the Moderate Resolution Imaging Spectroradiometer (MODIS) sensor were obtained from the NASA LAADS system as Level 1A and processed to Level 3 mapped images using the SeaDAS software.

3. Results and discussion

3.1. Autonomous front detection

The AUV conducted 23 transects across the front over nearly 4 days, generating an exceptionally high-resolution depiction of frontal structure and variability. To illustrate the effectiveness of the frontal detection method, one transect and its associated stratification parameter are shown in Fig. 2. The vehicle started from strongly stratified water in the upwelling shadow, where $\Delta Temp_{vert}$ was large. As the vehicle flew westward to the upwelling filament, $\Delta Temp_{vert}$ decreased. When $\Delta Temp_{vert}$ had fallen below $thresh_{\Delta Temp}$ for 5 consecutive yo–yo profiles, the AUV determined that it had passed the front and entered the weakly stratified water column, as marked by the blue triangle. Thus the AUV's

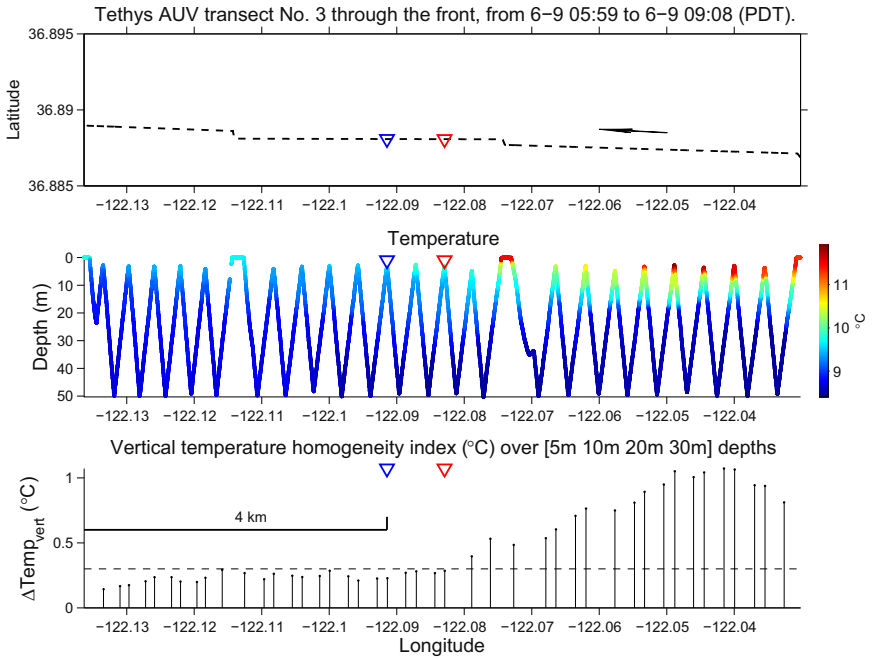

Fig. 2. Top panel: the horizontal track of one AUV transect from strongly stratified water to upwelling water. Middle panel: AUV-measured temperature on its yo–yo trajectory between surface and 50 m depth. Lower panel: $\Delta Temp_{vert}$ (i.e., VTHI), which was used as the AUV's real-time classifier for distinguishing between strongly and weakly stratified water columns. The classification threshold $thresh_{\Delta Temp} = 0.3$ °C is marked by the dashed line. The blue triangle marks the front detection location where the AUV determined that it had passed the front and entered the stratified water column; the red triangle marks the delay-corrected location of the front.

detection of the front came with a delay of 4 yo–yo profiles. The delay-corrected front location is marked by the red triangle. In all the remaining figures in this paper, only the delay-corrected front locations will be shown. The AUV continued flight into the upwelling water for 4 km to sufficiently cover the frontal zone, and then turned back to the strongly stratified upwelling shadow water. The horizontal distance between two adjacent yo–yo cusps was about 360 m, providing a spatial resolution about three times better than that of satellite SST (~1 km). More importantly, the AUV provided a high-resolution mapping of the subsurface structure of different water types across the front, which is beyond satellites' sensing capability but essential to understanding frontal processes.

3.2. Regional variability

Regional wind forcing is shown by the wind velocity measured at the NDBC buoy #46042, and hydrographic conditions in the outer bay are shown by temperature and salinity profiles measured at the M1 mooring (Fig. 3). Pacific Daylight Time (PDT) is

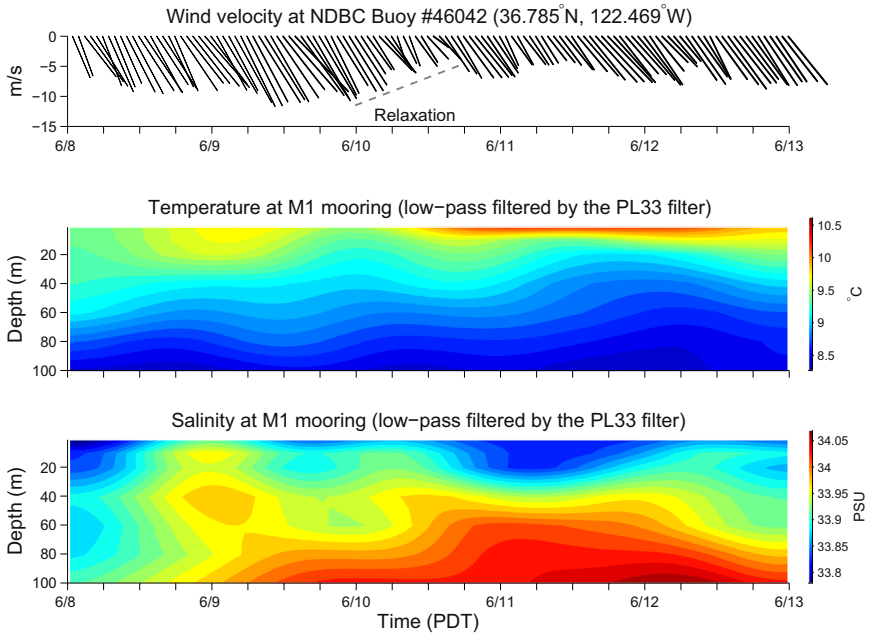

Fig. 3. Top panel: wind velocity measured at the NDBC buoy #46042. Middle and bottom panels: low-pass filtered temperature and salinity measured by the M1 mooring. See Fig. 1 for the buoy and mooring locations. (For interpretation of color in this figure, the reader is referred to the web version of this paper.)

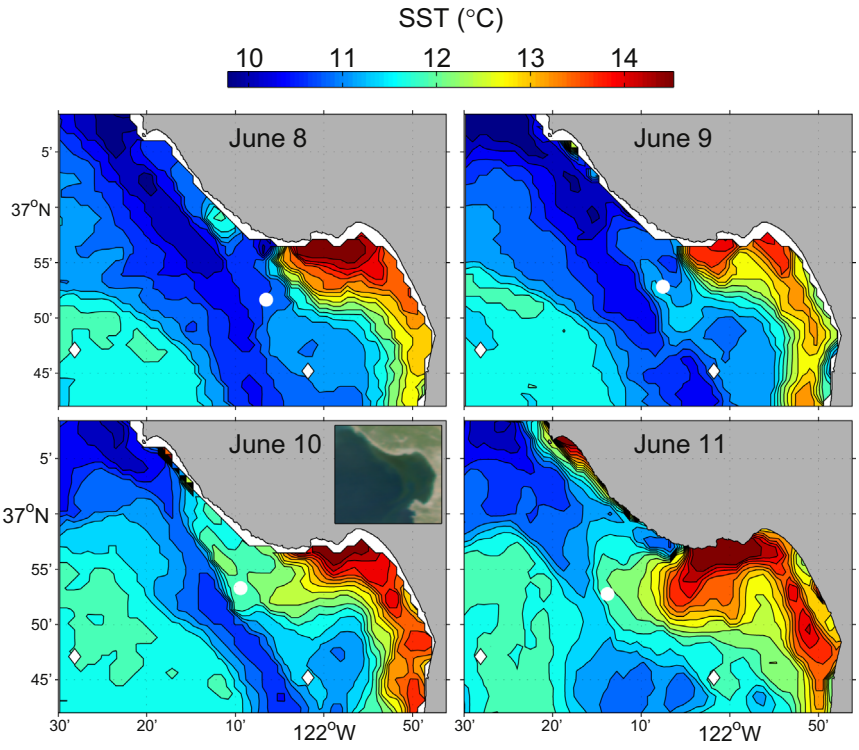

Fig. 4. Satellite SST of Monterey Bay on 6/8 21:09, 6/9 22:30, 6/10 22:09, 6/11 21:48 (PDT), 2012. The circles mark the AUV-tracked front locations within 4 h of each SST acquisition time. The MODIS ocean color at 6–10 12:54 (PDT) is shown in the inset in the lower-left panel. The NDBC buoy #46042 and the M1 buoy are marked by the left and right diamonds, respectively.

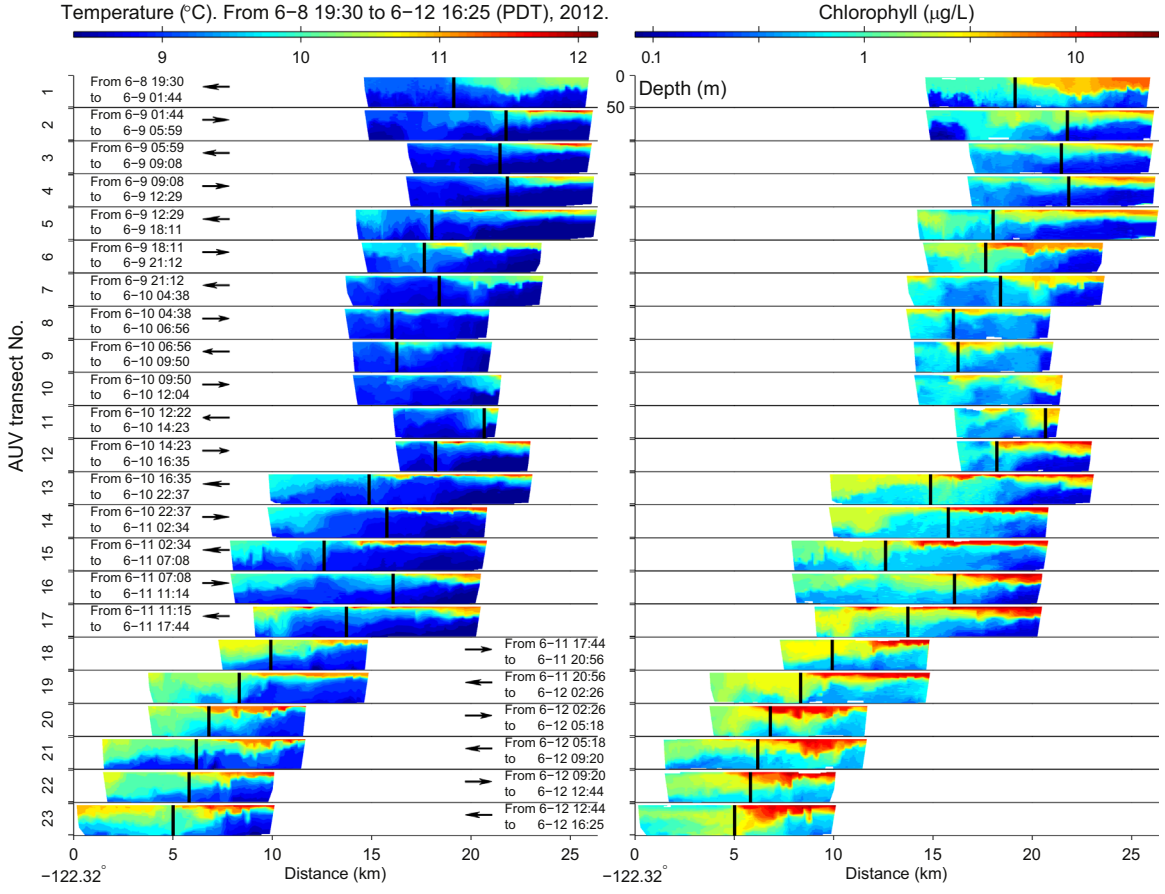

Fig. 5. AUV-measured temperature (left) and chlorophyll (right) from surface to 50 m depth on the 23 transects. The vehicle's flight direction is indicated by the arrow. The AUV-tracked front location is marked by the vertical bar. The time range of each transect is also noted. At the end of transect No. 10, the shore operator restarted the AUV mission (turning west). Post-experiment calculation of $\Delta Temp_{vert}$ shows that the end of this transect coincided with the front location.

used throughout this paper. From 6/8 to 6/10, southeastward (upwelling favorable) winds were strong (about 10 m/s), setting up an active upwelling phase. In this phase, low temperature and high salinity in the water column at the M1 mooring indicated impinging of an upwelling filament. On 6/10, the southeastward wind weakened to about 5 m/s, leading to a moderate relaxation phase. From 6/10 afternoon to 6/12, temperature increased and salinity decreased in the upper water column (above 30 m depth) at the M1 mooring, which is a typical response caused by both advection and local heating during a relaxation response (Rosenfeld et al., 1994; Breaker and Broenkow, 1994; Graham and Largier, 1997; Ramp et al., 2005; Shulman et al., 2010; Ryan et al., 2010b).

Satellite SST images (with overlaid AUV-tracked front locations) are shown in Fig. 4, and the satellite MODIS ocean color image of 6/10 is shown in an inset. From 6/8 to 6/9, an intense upwelling filament (characterized by low SST) extended southeastward from the Point Año Nuevo upwelling center to the mouth of the bay. On the eastern flank of the upwelling filament was the upwelling shadow water of high SST; on the western flank of the upwelling filament was the coastal transition zone (CTZ) water of intermediate SST (the CTZ refers to the zone between the near-shore upwelling region and the offshore California current (Huyer et al., 1991)). In the relaxation phase starting on 6/10, the upwelling filament weakened, signified by shrinking of the filament and also rising SST within the filament. Despite the coarse resolution of the MODIS ocean color image of 6/10 (due to the steep viewing angle), it unambiguously shows high chlorophyll (green color) in the bay (to the east of the front) in contrast to low chlorophyll level (blue color) to the west of the front. By 6/11, the upwelling filament receded further northwestward, and the upwelling shadow water came in direct contact with CTZ water. The SST images also show that on 6/10 and 6/11 the upwelling shadow water was advancing westward, signified by the westward expansion of the warm-SST area. While the satellite SST image series can provide synoptic surface descriptions of the front, the AUV autonomously tracked the front and revealed the subsurface properties and processes.

3.3. *Evolution of the AUV-tracked front*

The AUV-measured temperature and chlorophyll on all 23 transects are shown in Fig. 5. The AUV data samples on the yo–yo trajectory are interpolated to produce the sections in Figs. 5 and 8. The interpolation is performed by MATLAB® function TriScatteredInterp which uses Delaunay triangulation (de Berg et al., 2008). This time series shows that the temperature-stratification front

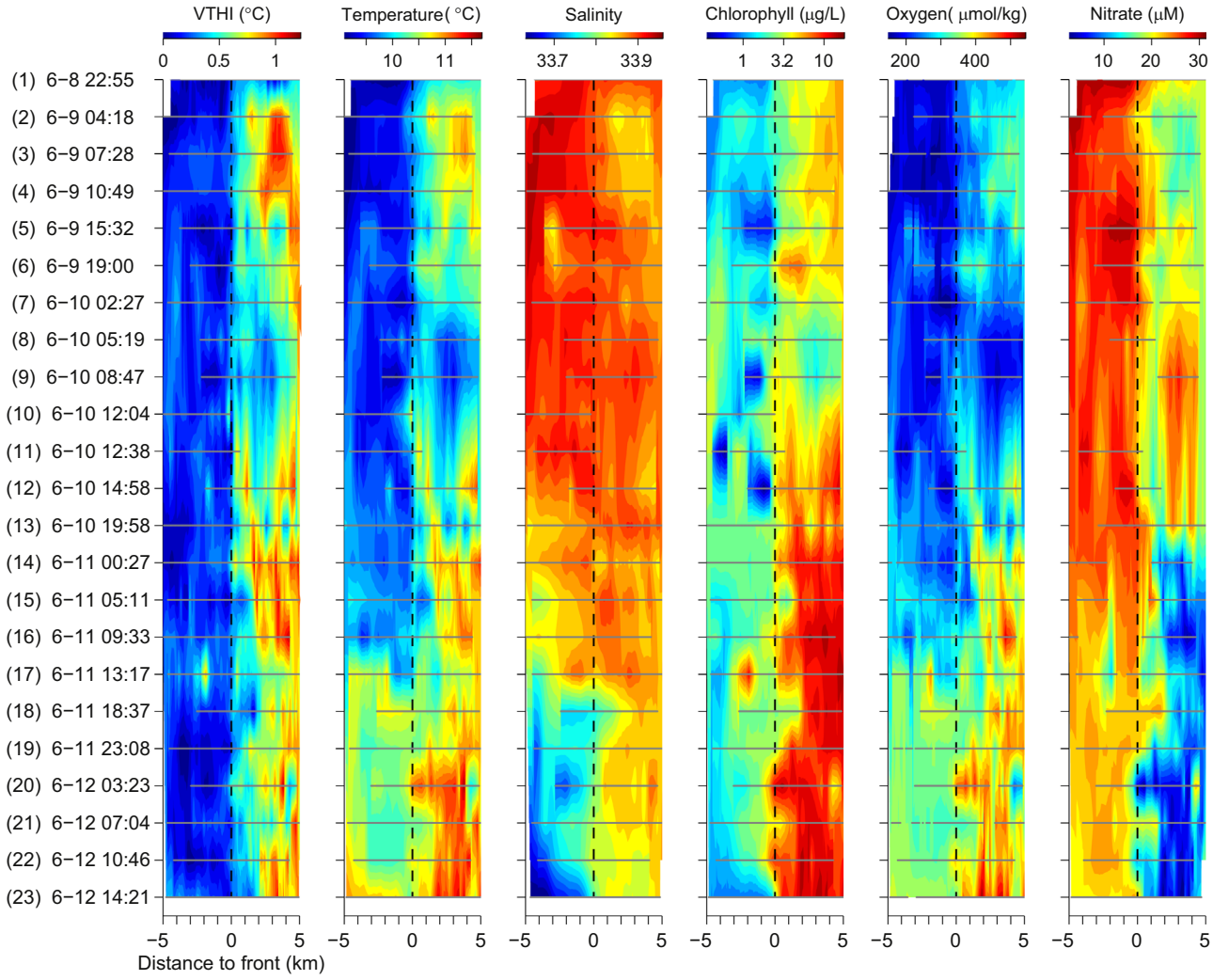

Fig. 6. Hovmöller diagram of upper water column properties on each AUV transect, which is plotted up to 5 km distance on each side of the AUV-tracked front location, and labeled with the transect number (in parentheses) and the front detection time. 1st panel: VTHI over [5 10 20 30]-meter depths. The front's location (marked by the dashed line) corresponds to the classification threshold *VTHI* = 0.3 °C. 2nd~6th panels: depth-averaged (in the upper 10 m) temperature, salinity, chlorophyll concentration, dissolved oxygen concentration, and nitrate, respectively. On each transect, the gray line marks the portion with AUV measurements, while the no-measurement portion is interpolated using AUV measurements from adjacent transects.

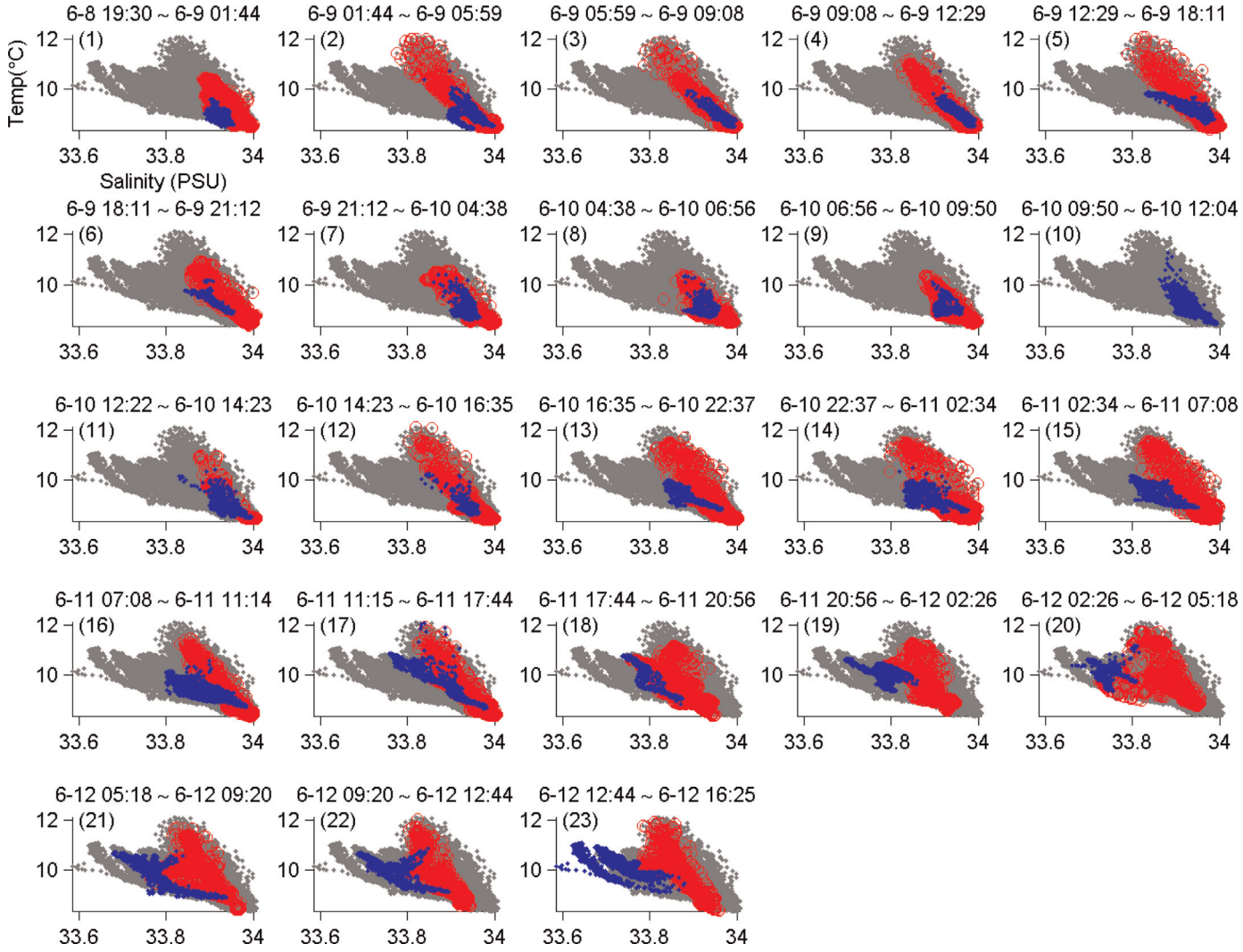

Fig. 7. *T–S* diagrams for the 23 AUV transects (transect number in parentheses). Data points on the inshore side of the front are in red; those on the offshore side of the front are in blue. The entire set of data points are in gray.

coincided with a biological front between phytoplankton-enriched water (in the upper 10–20 m) of the upwelling shadow east of the front and phytoplankton-poor water west of the front. On the inshore side of the front, a shallow layer of high temperature and high chlorophyll persisted, and the water column was strongly stratified. On the offshore side of the front, the shallow layer was not present, and the water column was weakly stratified in both temperature and chlorophyll. As shown in Fig. 4, the AUV-tracked front locations (circles) corresponded with the front locations evident in satellite SST. The westward advancement of the AUV-tracked front during the relaxation phase (starting on 6/10) was consistent with the satellite SST observations.

Fig. 5 shows that the upper water column properties (in the upper 10 m) contrasted across the front. Hence we use depth-averaged (in the upper 10 m) values of each property (temperature, salinity, chlorophyll, dissolved oxygen, and nitrate) to examine biogeochemistry variability across the front (Fig. 6). In this Hovmöller diagram, each transect is referenced to the front location (i.e., taking the front location as the origin on the distance axis) to represent the evolution of biogeochemical properties in the moving reference frame of the front itself. On each transect, the gray line marks the portion with AUV measurements, while the no-measurement portion is interpolated using AUV measurements from adjacent transects. The interpolation is again performed by MATLAB® function TriScatteredInterp which uses Delaunay triangulation.

Temperature stratification (i.e., VTHI in the first panel of Fig. 6) was a consistent identifier of the front throughout the four-day tracking. However, the biogeochemical nature of the water types to either side of the front changed dramatically as regional circulation responded to relaxation of upwelling.

In the active upwelling phase from 6/8 to 6/10, an intense upwelling filament was extending southeastward from the Point Año Nuevo upwelling center to the mouth of the bay. The AUV tracked the front between the upwelling shadow (on the inshore side) and the upwelling filament (on the offshore side). The upwelling filament water was characterized by low temperature, chlorophyll, and dissolved oxygen, and high salinity and nitrate. Phytoplankton growth was not established in this newly upwelled water column, so chlorophyll and oxygen were not elevated, and nitrate remained high. In the upwelling shadow water, the shallow layer of high chlorophyll was accompanied by low nitrate and high dissolved oxygen, likely signifying shallow-water phytoplankton communities consuming nitrate and producing oxygen. In this water type the appearance of anomalously cool, saline water with elevated nitrate and low chlorophyll and oxygen is consistent with influx of recently upwelled water into the upwelling shadow.

In the relaxation phase from 6/10 to 6/12, the upwelling

filament waned, and the upwelling shadow advanced westward to come in direct contact with the CTZ water. The AUV tracked the front between the upwelling shadow water (on the inshore side) and the relatively fresh CTZ water (on the offshore side). The inshore water type warmed, consistent with local heating. From 6/11 noon through the end of the time series, the inshore water type also freshened slightly near the front, consistent with cross-frontal exchange (examined in Section 3.4). The most significant biogeochemical changes were increased chlorophyll concentrations on the inshore side of the front (up to one order of magnitude higher than in the active upwelling phase) and associated increase in oxygen and decrease in nitrate. These changes may have resulted from both advective and local processes. The role of advection is supported by the satellite SST time series (Fig. 4), which shows that warm water moved from the northernmost region of the bay southwestward across the AUV section (36.9°N) during the relaxation response. Further, this warm near-coastal water was enriched in phytoplankton (see the MODIS image inset in Fig. 4). A possible local process enhancing phytoplankton biomass is accumulation of motile phytoplankton in horizontally convergent flow at the front (Ryan et al., 2010b, 2010a). However, the AUV transect series shows no evidence of diurnal vertical migration by the phytoplankton (Fig. 5), thus the role of this process is not supported. A second possible local process is enhancement of phytoplankton growth conditions caused by local stratification following upwelling nutrient influx. Examination of this local process would require in situ productivity measurements on a truly Lagrangian platform (e.g., a drifter) that follows a tagged water mass. The AUV was tracking the front, rather than a tagged water mass. Hence the AUV-measured biogeochemical variabilities were combinations of advected water properties and local growth. The experiment was not designed for (and not sufficient for) investigating the local growth process, but aiming at persistently observing the evolution of water properties on both sides of the front. However, high-resolution observations from the AUV did indicate cross-frontal exchange processes during the upwelling phase, consistent with enhancement of growth conditions inshore of the front (Section 3.4).

The change of water types is also demonstrated by the temperature–salinity (T–S) diagrams for the 23 AUV transects (Fig. 7). Data points on the inshore side of the front are colored red; those on the offshore side of the front are colored blue. The entire set of data points are in gray. On each transect, the offshore-side cluster (in blue) had a much smaller spread than the inshore-side cluster (in red), because the water column was relatively homogeneous on the offshore side of the front. From 6/8 to 6/10 (the active upwelling phase), the blue cluster was characterized by low temperature and high salinity, indicating the upwelling filament water. From 6/10 to 6/12 (the relaxation phase), the blue cluster "migrated" to the upper-left (higher temperature and lower salinity), indicating the offshore-side water type changing to warmer and fresher CTZ water. The T-S spread of the red cluster remained large, indicating persistent stratification of the upwelling shadow water. It is noted that the highest salinity water was found inshore of the front during the active upwelling phase. In Section 3.4, it will be shown that this highest salinity water lay below 30 m depth inshore of the front, as a result of stirring of the upwelled water into the upwelling shadow beneath its warm upper layer.

3.4. Fine-scale mixing processes revealed by AUV's high-resolution measurements

Vertical thermal stratification remained a consistent identifier of water types and the front between them, yet cross-frontal exchange was evident in depth-averaged biogeochemical properties (Fig. 6). These indications of exchange and associated stirring and mixing of water types are examined with full-resolution water column sections from different phases of the upwelling to relaxation transition (Fig. 8). For this purpose, salinity serves as a conservative tracer of water types and is presented relative to temperature (used to compute VTHI) and density. Note that ocean circulation is three-dimensional, while the AUV transects are two-dimensional (cross-front and vertical). Nonetheless, the AUV transects captured 2-D "slices" of the 3-D circulation. They

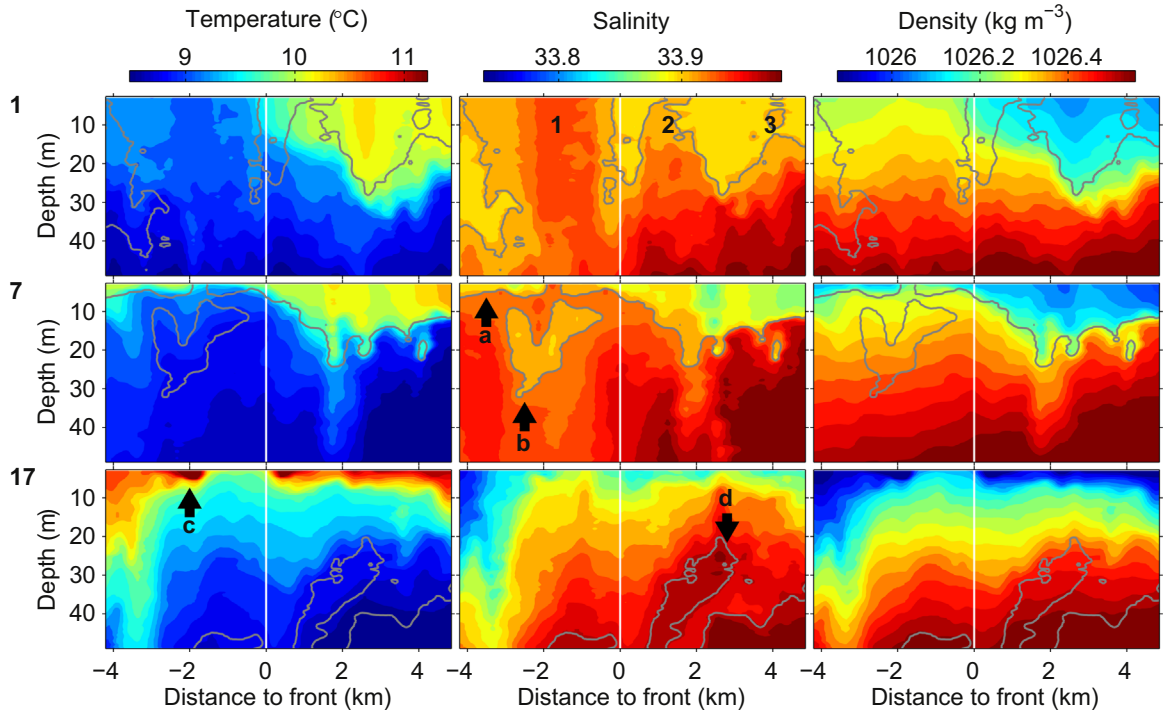

Fig. 8. AUV-measured temperature, salinity, and density measured on transects 1, 7 and 17 (see text for descriptions of the marked features). On each transect, the vertical white bar marks the AUV-tracked front location. A distance range of about 4 km to each side of the front is plotted.

revealed the mixing processes as seen on those 2-D slices, as described as follows.

During the upwelling phase, the front was between the warm upwelling shadow water (on the inshore side) and the cold and salty upwelled water (on the offshore side). The AUV data revealed a series of salinity anomalies indicating lateral stirring and mixing. The highest salinity in the upper 20 m was within the upwelling plume, immediately offshore of the front (Fig. 8, transect 1, label 1 in salinity panel). Two high-salinity features were inshore of the front (labels 2 and 3), separated by lower salinity water. This interleaving of salinity anomalies is consistent with stirring of the high salinity anomaly, which originated from upwelling, into the upwelling shadow. The weakening signal of the high-salinity anomaly between the presumed origin in the upwelling filament (label 1) and the inner bay (label 3) is consistent with mixing. The highest salinity water was inshore of the front, below 30 m depth, suggesting that upwelled water was entering the upwelling shadow beneath its warm upper layer and beneath the surface manifestation of the front.

Later in the upwelling phase, relatively high-salinity water was present across the entire section, and the most saline water occupied a greater proportion of the upwelling shadow below 10 m depth (Fig. 8, transect 7). This is consistent with increasing influence of upwelled water on the study region. Coincident warm, fresh anomalies above 7 m depth offshore of the front indicates offshore transport of shallow upwelling shadow water (arrow a). A low-salinity subsurface patch offshore of the front, between 10 m and 30 m depths, coincided with relatively cool water (arrow b), thus its origin was probably offshore of the upwelling filament rather than the warm upwelling shadow.

Following relaxation of upwelling, the front was between the upwelling shadow water (on the inshore side) and CTZ water (on the offshore side) that was colder and fresher than the upwelling shadow water. On transect 17, the AUV detected multiple features indicative of stirring and mixing, as shown in Fig. 8. In shallow water above 7 m depth, the very warm anomaly near 2 km offshore of the front (arrow c) suggests export of upwelling shadow water that was also strongly temperature stratified. This is supported by the fact that this shallow patch was associated with high chlorophyll and oxygen, and low nitrate (Fig. 6, transect 17), all features of the upwelling shadow water. Inshore of the front high-salinity water shoaled. However, the weakening of upwelling that was occurring would not cause shoaling of isohalines, suggesting the role of vertical mixing during the relaxation response. An isolated patch of high salinity water extended about 2 km horizontally and 30 m vertically, across isopycnals (arrow d), consistent with subsurface stirring and mixing of the high salinity water that originated from deeper water.

4. Conclusions

In June 2012, the Tethys AUV ran an autonomous algorithm to track a temperature stratification front in the Monterey Bay upwelling system, thereby providing high-resolution observations of the evolution of the frontal zone and fine-scale mixing processes. Through 23 frontal crossings in four days, the AUV tracked the front between the strongly stratified and phytoplankton-enriched upwelling shadow water, and the weakly stratified and phytoplankton-poor water, through an active upwelling phase and a succeeding moderate relaxation phase. The water type on the offshore side of the front began as newly upwelled water during the active upwelling phase, but changed to relatively fresh CTZ water during the succeeding relaxation phase. The biogeochemical nature of the water types to either side of the front changed in response to relaxation of upwelling. The most significant biogeochemical changes were increased chlorophyll concentrations on the inshore side of the front and associated increase in oxygen and decrease in nitrate. This was consistent with enhanced productivity in the upwelling shadow during the relaxation response, marked by consumption of nitrate and production of oxygen. Enhanced productivity would be expected from nutrient supply during the upwelling phase followed by warming and stratification during the relaxation phase. The AUV's high-resolution measurements also revealed fine-scale exchange processes across the front. The AUV's four-day front tracking has thus provided an unprecedentedly detailed depiction of the frontal zone from active upwelling to relaxation.

Acknowledgments

This work was supported by the David and Lucile Packard Foundation. The authors thank Thomas Hoover, Brian Kieft, Brett Hobson, Robert McEwen, Denis Klimov, and Ed Mellinger for helping with the Tethys AUV operations. The authors are thankful to Reiko Michisaki, Marguerite Blum, and Timothy Pennington for providing lab analysis results of ship deck CTD-rosette water samples for correcting AUV measurements, and to Leslie Rosenfeld for the help on using the PL33 low-pass filter.

References

Barber, R., Smith, R.L., 1981. Coastal upwelling ecosystems. In: Longhurst, A.R. (Ed.), Analysis of Marine Ecosystems. Academic Press, London, pp. 31–68.

Beardsley, R.C., Limeburner, R., Rosenfeld, L.K., 1985. Introduction to the CODE-2 moored array and large-scale data report. Technical Report 85-35, Woods Hole Oceanographic Institution.

Bellingham, J.G., Hobson, B., Godin, M.A., Kieft, B., Erikson, J., McEwen, R., Kecy, C., Zhang, Y., Hoover, T., Mellinger, E., 2010a. A small, long-range AUV with flexible speed and payload. Ocean Sciences Meeting, Abstract MT15A-14.

Bellingham, J.G., Zhang, Y., Kerwin, J.E., Erikson, J., Hobson, B., Kieft, B., Godin, M., McEwen, R., Hoover, T., Paul, J., Hamilton, A., Franklin, J., Banka, A., 2010b. Efficient propulsion for the Tethys long-range autonomous underwater vehicle. IEEE AUV 2010, pp. 1–6.

de Berg, M., Cheong, O., van Kreveld, M., Overmars, M., 2008. Computational geometry: algorithms and applications. 3rd ed., Chapter 9, Springer-Verlag, Berlin, pp. 191–218.

Breaker, L.C., Broenkow, W.W., 1994. The circulation of Monterey Bay and related processes. Oceanogr. Mar. Biol.: Annu. Rev. 32, 1–64.

Graham, W.M., Field, J.G., Potts, D.C., 1992. Persistent "upwelling shadows" and their influence on zooplankton distributions. Mar. Biol. 114, 561–570.

Graham, W.M., Largier, J.L., 1997. Upwelling shadows as nearshore retention sites: the example of northern Monterey Bay. Cont. Shelf Res. 17, 509–532.

Harvey, J.B.J., Ryan, Marin III, R., Preston, C.M., Alvarado, N., Scholin, C.A., Vrijenhoek, R.C., 2012. Robotic sampling, in situ monitoring and molecular detection of marine zooplankton. J. Exp. Mar. Biol. Ecol. 413, 60–70.

Hobson, B., Bellingham, J.G., Kieft, B., McEwen, R., Godin, M., Zhang, Y., 2012. Tethys-class long range AUVs—extending the endurance of propeller-driven cruising AUVs from days to weeks. In: Proceedings of IEEE on AUV'2012, pp. 1–8.

Huyer, A., Kosro, P.M., Fleischbein, J., Ramp, S.R., Stanton, T., Washburn, L., Chavez, F. P., Cowles, T.J., Pierce, S.D., Smith, R.L., 1991. Currents and water masses of the coastal transition zone off northern California, June to August 1988. J. Geophys. Res. 96, 14809–14831.

Jessup, D.A., Miller, M.A., Ryan, J.P., Nevins, H.M., Kerkering, H.A., Mekebri, A., Crane, D.B., Johnson, T.A., Kudela, R.M., 2009. Mass stranding of marine birds caused by a surfactant-producing red tide. PLoS ONE 4, e4550.

Pennington, J.T., Chavez, F.P., 2000. Seasonal fluctuations of temperature, salinity, nitrate, chlorophyll and primary production at station H3/M1 over 1989-1996 in Monterey Bay, California. Deep-Sea Res. II 47, 947–973.

Ramp, S.R., Paduan, J.D., Shulman, I., Kindle, J., Bahr, F.L., Chavez, F., 2005. Observations of upwelling and relaxation events in the northern Monterey Bay during August 2000. J. Geophys. Res. 110, C07013.

Rosenfeld, L.K., Schwing, F.B., Garfield, N., Tracy, D.E., 1994. Bifurcated flow from an upwelling center: a cold water source for Monterey Bay. Cont. Shelf Res. 14, 931–964.

Ryan, J., Harvey, J.B.J., Zhang, Y., Woodson, C.B., 2014a. Distributions of invertebrate larvae and phytoplankton in a coastal upwelling system retention zone and peripheral front. J. Exp. Mar. Biol. Ecol. 459, 51–60.

Ryan, J.P., 2011. CANON June experiment overview. Technical Report, Monterey Bay Aquarium Research Institute.

Ryan, J.P., Fischer, A.M., Kudela, R.M., McManus, M.A., Myers, J.S., Paduan, J.D.,

Ruhsam, R.S., Woodson, C.B., Zhang, Y., 2010b. Recurrent frontal slicks of a coastal ocean upwelling shadow. J. Geophys. Res. 115.
Ryan, J.P., Gower, J.F.R., King, S.A., Bissett, W.P., Fischer, A.M., Kudela, R.M., Kolber, Z., Mazzillo, F., Rienecker, E.V., Chavez, F.P., 2008a. A coastal ocean extreme bloom incubator. Geophys. Res. Lett. 35, L12602.
Ryan, J.P., Greenfield, Marin III, R., Preston, C., Roman, B., Jensen, S., Pargett, D., Birch, J., Mikulski, C., Doucette, G., Scholin, C., 2011. Harmful phytoplankton ecology studies using an autonomous molecular analytical and ocean observing network. Limnol. Oceanogr. 56, 1255–1272.
Ryan, J.P., McManus, M.A., Kudela, R., Artigas, M.L., Bellingham, J.G., Chavez, F.P., Doucette, G., Foley, D., Godin, M., Harvey, J.B.J., Marin III, R., Messie, M., Mikulski, C., Pennington, T., Py, F., Rajan, K., Shulman, I., Wang, Z., Zhang, Y., 2014b. Boundary influences on HAB phytoplankton ecology in a stratification-enhanced upwelling shadow. Deep-Sea Res. II 101, 63–79.
Ryan, J.P., McManus, M.A., Paduan, J.D., Chavez, F.P., 2008b. Phytoplankton thin layers caused by shear in frontal zones of a coastal upwelling system. Mar. Ecol. Prog. Ser. 354, 21–34.
Ryan, J.P., McManus, M.A., Sullivan, J.M., 2010b. Interacting physical, chemical and biological forcing of phytoplankton thin-layer variability in Monterey Bay, California. Cont. Shelf Res. 30, 7–16.
Shulman, I., Anderson, S., Rowley, C., DeRada, S., Doyle, J., Ramp, S., 2010. Comparisons of upwelling and relaxation events in the Monterey Bay area. J. Geophys. Res. 115, C06016.
Woodson, C.B., Barth, J.A., Cheriton, O.M., McManus, M.A., Ryan, J.P., Washburn, L., et al., 2011. Observations of internal wave packets propagating along-shelf in northern Monterey Bay. Geophys. Res. Lett. 38, L01605.
Woodson, C.B., McManus, M.A., Tyburczy, J.A., Barth, J.A., Washburn, L., Caselle, J.E., Carr, M.H., Malone, D.P., Raimondi, P.T., Menge, B.A., Palumbi, S.R., 2012. Coastal fronts set recruitment and connectivity patterns across multiple taxa. Limnol. Oceanogr. 57, 582–596.
Woodson, C.B., Washburn, L., Barth, J.A., Hoover, D.J., Kirincich, A.R., McManus, M.A., Ryan, J.P., Tyburczy, J., 2009. Northern Monterey Bay upwelling shadow front: observations of a coastally and surface-trapped buoyant plume. J. Geophys. Res. 114.
Zhang, Y., Godin, M.A., Bellingham, J.G., Ryan, J.P., 2012a. Using an autonomous underwater vehicle to track a coastal upwelling front. IEEE J. Ocean. Eng. 37, 338–347.
Zhang, Y., Ryan, J.P., Bellingham, J.G., Harvey, J.B.J., McEwen, R.S., 2012b. Autonomous detection and sampling of water types and fronts in a coastal upwelling system by an autonomous underwater vehicle. Limnol. Oceanogr.: Methods 10, 934–951.